THE JOURNAL OF BIOLOGICAL CHEMISTRY VOL. 285, NO. 50, pp. 39029–39038, December 10, 2010

The Active Site of Oligogalacturonate Lyase Provides Unique Insights into Cytoplasmic Oligogalacturonate β-Elimination*

Received for publication, June 11, 2010, and in revised form, August 17, 2010 Published, JBC Papers in Press, September 17, 2010, DOI 10.1074/jbc.M110.153981

D. Wade Abbott[‡1], **Harry J. Gilbert**[‡2], **and Alisdair B. Boraston**[§3]

From the [‡]*Complex Carbohydrate Research Center, University of Georgia, Athens, Georgia 30602 and the* [§]*Department of Biochemistry and Microbiology, University of Victoria, Victoria, British Columbia V8W 3P6, Canada*

Oligogalacturonate lyases (OGLs; now also classified as pectate lyase family 22) are cytoplasmic enzymes found in pectinolytic members of Enterobacteriaceae, such as the enteropathogen *Yersinia enterocolitica*. OGLs utilize a β-elimination mechanism to preferentially catalyze the conversion of saturated and unsaturated digalacturonate into monogalacturonate and the 4,5-unsaturated monogalacturonate-like molecule, 5-keto-4-deoxyuronate. To provide mechanistic insights into the specificity of this enzyme activity, we have characterized the OGL from *Y. enterocolitica*, *Ye*OGL, on oligogalacturonides and determined its three-dimensional x-ray structure to 1.65 Å. The model contains a Mn^{2+} atom in the active site, which is coordinated by three histidines, one glutamine, and an acetate ion. The acetate mimics the binding of the uronate group of *galactourono*-configured substrates. These findings, in combination with enzyme kinetics and metal supplementation assays, provide a framework for modeling the active site architecture of OGL. This enzyme appears to contain a histidine for the abstraction of the α-proton in the −1 subsite, a residue that is highly conserved throughout the OGL family and represents a unique catalytic base among pectic active lyases. In addition, we present a hypothesis for an emerging relationship observed between the cellular distribution of pectate lyase folding and the distinct metal coordination chemistries of pectate lyases.

The distal gut microbiota of monogastric animals is a bioreactor consisting of 10–100 trillion bacteria from up to a thousand different species (1, 2). This diverse community, referred to as the "forgotten organ" (3), unlocks the rich source of chemical energy present within the glycosidic bonds of plant cell wall polysaccharides ingested as part of the host diet. These potential substrates are indigestible by the full repertoire of glycoside hydrolases and lyases encoded within the human genome. Consistent with this biological role, analysis of the gut metagenome has revealed an enormous arsenal of enzymes active in the modification and utilization of plant cell wall polysaccharides (2, 4). Recently, using transcriptomic technology, some of the catabolic strategies employed by the model gut microbe *Bacteroides thetaiotaomicron* have illuminated the dynamic relationship that exists between dietary regime, host glycan assemblies, and the composition of the microbiota (2, 5, 6). However, how these induced enzymes operate at the biochemical level and deconstruct complex target substrates still remains poorly understood.

By comparison with the natural flora, the processes by which enteropathogenic bacterial populations interact within this dynamic microecosystem has received significantly less attention in the literature. In particular, the mechanisms by which pathogens compete for nutrients during infection, colonization, and disease progression remain to be determined. At the turn of this century, hexuronide transport and utilization systems responsive to KdgR (2-keto-3-deoxygluconate repressor protein) were identified in the genomes of several gut pathogens (7, 8). These observations have provided a platform for exploring the capability of infectious agents, such as *Yersinia enterocolitica*, to metabolize pectic plant cell wall polysaccharides.

Pectin is chemically the most complex carbohydrate found in nature. It is located within the primary cell walls and middle lamella of most terrestrial plants, indicating that it is involved in intercellular interactions (9). Pectin is a negatively charged and heavily hydrated polysaccharide that cross-links the load-bearing cellulosic components of the cell wall. This class of structural carbohydrate is defined by the presence of a galacturonic acid (GalA)[4] component within its backbone, interconnected through α-1,4 linkages. The abundance and composition of its decorations, however, vary significantly, which forms the basis for its classification into three major subtypes: homogalacturonan, rhamnogalacturonan I, and rhamnogalacturonan II (9). The identity of these side chains and the inherent charge status of uronate groups in homogalacturonan are critical factors for regulating the function of distinct pectic polysaccharides during various phytophysiological events. For example, methylesterification of homogalacturonan, which neutralizes the GalA subunits, regulates dynamic and reversible packing of fibers in a process called "gellation." (10)

* This work was supported by grants from the Georgia Research Alliance (to H. J. G.) and the Natural Sciences and Engineering Research Council of Canada (to A. B. B.).

The atomic coordinates and structure factors (code 3PE7) have been deposited in the Protein Data Bank, Research Collaboratory for Structural Bioinformatics, Rutgers University, New Brunswick, NJ (http://www.rcsb.org/).

[1] To whom correspondence may be addressed: Complex Carbohydrate Research Center, University of Georgia, 315 Riverbend Rd., Athens, Georgia 30602. E-mail: wabbott@ccrc.uga.edu.

[2] A Georgia Research Alliance Eminent Scholar in Bioenergy.

[3] A Canada Research Chair in Molecular Interactions and a Michael Smith Foundation for Health Research Career Scholar. To whom correspondence may be addressed: Dept. of Biochemistry and Microbiology, University of Victoria, P.O. Box 3055 STN CSC, Victoria, British Columbia V8W 3P6, Canada. E-mail: boraston@uvic.ca.

[4] The abbreviations used are: GalA, galacturonic acid; $GalA_2$, digalacturonate; $GalA_3$, trigalacturonate; PL, pectate lyase; OGL, oligogalacturonate lyase; KDG, 2-keto-3-deoxygluconate; r.m.s., root mean square; DKI, 5-keto-4-deoxyuronate.

The pectic network is an energy-rich substrate targeted for catabolism by pectinolytic microorganisms. This complex carbohydrate is an amenable substrate, when compared with crystalline structural polysaccharides, due to its polarity, hydration level, and flexibility. Extracellular depolymerization of pectin is associated with the activity of secreted pectinases from dedicated phytopathogens and saprophytes. Conversely, the intracellular stages of pectic utilization, involving reactions that convert pectic fragments released by upstream extracellular processes into smaller metabolites, are common to a wider variety of pectinolytic bacteria. Recently, we reported several advances toward understanding the molecular basis for polygalacturonate depolymerization and transport using the enteropathogen *Y. enterocolitica* as a model organism (see Ref. 11 for a recent review) (Fig. 1). The mechanisms governing the intracellular conversion of oligogalacturonides into downstream metabolites remain less understood.

The highly conserved cytosolic pathway was first documented in *Erwina chrysanthemi* (now renamed *Dickeya dadantii Ech586*) using biochemical and genetic approaches in the 1980s and 1990s (see Ref. 12 for an extensive review) (Fig. 1). In the initial stages, intracellular di- and trigalacturonides are processed into saturated monogalacturonate (GalA) and a 4,5-unsaturated GalA-like monosaccharide (DKI; 5-keto-4-deoxyuronate) by the combined activities of an *exo*-acting family 2 pectate lyase (referred to as *Ye*PL2B in *Y. enterocolitica* (13, 14)) and oligogalacturonate lyase (*Ye*OGL/*Ye*PL22 in *Y. enterocolitica*), a novel lyase family preferentially active on digalacturonides (14) (see Fig. 2 for a generalized reaction mechanism). GalA and DKI then undergo a short parallel series of chemical modifications culminating in the production of 2-keto-3-deoxygluconate (KDG), the central metabolite in the regulation of pectin-inducible genes. Despite this understanding of the pathway, the molecular processes that define substrate recognition and catalytic mechanism within each stage of the intracellular catabolism of pectic fragments still remain to be defined.

In this study, we have explored in further detail the mechanism of oligogalacturonate lyase (OGL) activity by using the oligogalacturonate lyase from *Y. enterocolitica*, *Ye*OGL. These findings illuminate several features of oligogalacturonide β-elimination, which is distinct from polysaccharide lyases, define a new family of cytoplasmic pectate lyase within the Carbohydrate-Active Enzymes Database (CAZy; available on the World Wide Web) (15), and present a hypothesis to explain the relationship between cellular localization of pectate lyases and the coordination of distinct metal cofactors.

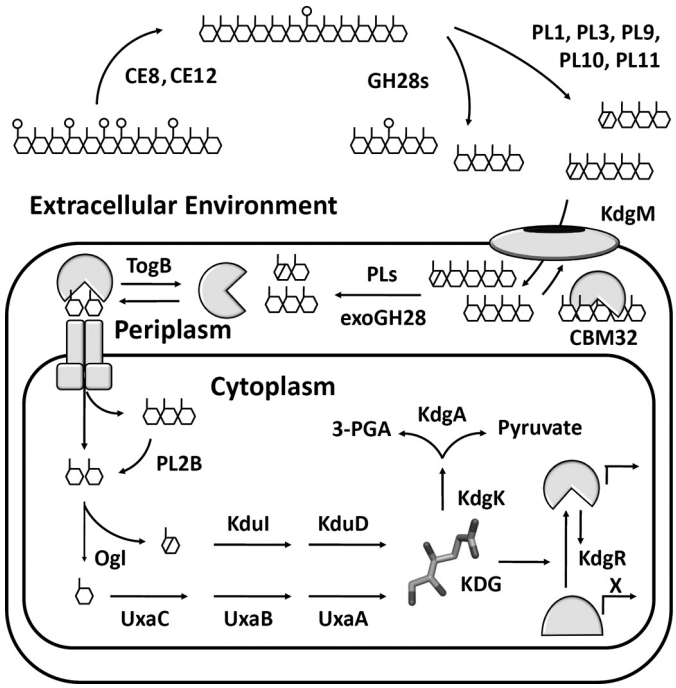

FIGURE 1. **General pectin degradation pathway found in pectinolytic bacteria from Enterobacteraciae (11).** Extracellular pectin depolymerization is primarily restricted to phytopathogens and involves a consortium of enzymes that liberate fragments from the highly polymerized pectic network within the plant cell wall. Pectinases involved in these processes include PLs, polygalacturonases (GH28s), and carbohydrate esterases (CE8). Products diffuse into the periplasmic space through anionic porins belonging to the KdgM family, where a specialized collection of proteins operates to retain and concentrate (CBM32) and process pectic substrates into mono-, di-, and trisaccharides (PLs and exoGH28). Intracellular transport of oligogalacturonides is facilitated by integral membrane systems, including the ATP-dependent transporter TogMNAB. Within the cell, pectin catabolism remains poorly understood at the structural level; however, a pathway has been established based upon genetics, biochemistry, and comparative genomics (7, 12). There are two branches of metabolism dedicated to saturated monogalacturonate (GalA; UxaA, UxaB, and UxaC), and unsaturated monogalacturonate (DKI; KduI and KduD), the product of pectate lyases. These pathways converge to produce KDG, which is the inducer of KdgR, a repressor protein that regulates the expression of virtually every pectin utilization gene known. KDG is converted into the metabolites 3-phosphoglyceraldehyde and pyruvate by a two-step phosphorylation and hydrolysis reaction path catalyzed by KdgK and KdgA, respectively.

EXPERIMENTAL PROCEDURES

Molecular Cloning, Gene Expression, Protein Production, and Purification—Recombinant *Ye*OGL was prepared according to techniques described previously (16). Briefly, the full-length gene locus *YE*1876 (*ogl*), which encodes a 388-amino acid 44.2-kDa protein, was amplified by polymerase chain reaction from *Y. enterocolitica* subsp. *enterocolitica 8081* genomic DNA (ATCC number 23715^{TM}) using forward (ATATGCTAGCATGGCTAAAGGTAAACAAATCCCCCTGA) and reverse (TATACTCGAGCTATTTCCAGACTGATTCAGGCAATGTGGCT) oligonucleotide primers. The gene fragment was restricted using engineered NheI 5′ and XhoI 3′ sites and ligated into pET28a digested with complementary restriction enzymes to create the expression vector pET28-*Ye*OGL. *Ye*OGL encoded by pET28-*Ye*OGL contains a thrombin-cleavable N-terminal His_6 tag. The construct was transformed into chemically competent BL21-pLysS (DE3) cells, and 1.0-liter cultures of LB were grown supplemented with 50 μg/ml kanamycin. When cultures reached an optical density of ~0.6 (at 600 nm), the temperature was decreased to 16 °C, and recombinant gene expression was induced by the addition of isopropylthiogalactopyranoside to a final concentration of 0.2 mM. Induced cultures were incubated overnight with shaking. Cells were then pelleted, resuspended in binding buffer (500 mM NaCl, 20 mM Tris-HCl, pH 8.0), and lysed by French press. The lysate was clarified by centrifugation at 17,000 × *g* for 45 min, and the supernatant was loaded directly onto a nickel-charged immobilized metal affinity chromatography column. After extensive washing with binding buffer, bound polypeptides were eluted by a stepwise 5–500 mM imidazole gradient in bind-

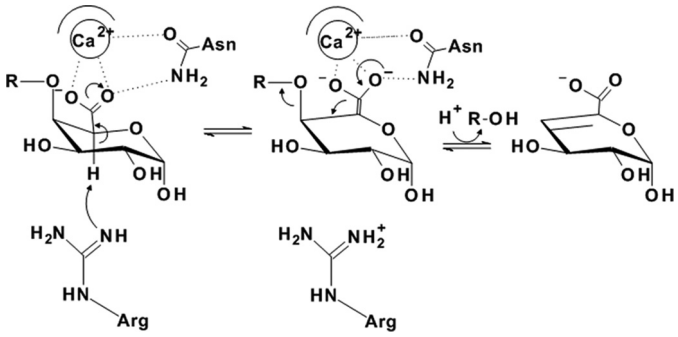

FIGURE 2. **General β-elimination reaction mechanism for catalysis by pectate lyases.** α1,4-Linked galacturonate substrates adopting the relaxed $^4C_1$ chair conformation present the ideal geometry for an *anti* periplanar transelimination with the C5 hydrogen and C4 hydroxyl group both orientated in axial configurations. The rate-limiting step is the acidification and deprotonation of C5, a process that is facilitated by the effects of the electrophilic uronate group, catalytic divalent metals, and localized basic residues within the active site, which draw charge from the C5 carbon and increase the reactivity of its lone hydrogen atom. Abstraction occurs via general base attack by an arginine (family 1, 2, 3, and 10) or lysine (family 9) (43), the high pK_a of these residues accounting for the basic pH optima observed across the PL landscape. Recently, the contributions of an ancillary lysine in family 1 PLs and asparagines in family 9 have been proposed to influence the catalytic rate by stabilizing the enolate-enolate intermediate (45). These residues have been implicated in hydrogen donation and/or bonding to the nascent oxyanion of the uronate group following electron transfer to the transient double bond between C5 and C6. Decomposition of the intermediate occurs by protonation of the scissile glycosidic oxygen and elimination of the axial O4 by electron shuttling from the C5–C6 bond to the C4–C5 bond of the sugar ring. This unsaturation distorts the relaxed chair structure of the pyranose because the trigonal planar geometry of C4 and C5 results in migration of C4 into the plane of C2, C3, and C5. The substrate is shown is a disaccharide, with the R-group depicting a second GalA or DKI molecule (note the Asn residue shown may be equivalent to Gln^{350}).

TABLE 1
Crystallographic statistics for the structure of *Ye*OGL

Data collection	
Space group	$P2_12_12_1$
Cell dimensions	
a (Å)	66.65
b (Å)	75.51
c (Å)	78.51
α (degrees)	90.00
β (degrees)	90.00
γ (degrees)	90.00
Resolution (Å)	30.00-1.65
R_{merge}	0.085 (0.35)
$I/\sigma I$	14.9 (4.0)
Completeness (%)	97.7 (85.5)
Multiplicity	6.8 (4.4)
Average mosaicity	0.44
Refinement	
Resolution (Å)	35.42-1.65 (1.69-1.65)
No. of reflections	44,824
R_{work}/R_{free}	0.18/0.20
No. of atoms	3527
Protein	3019
Acetate/ion	4/3
Water	497
B-Factors (Å^2)	
Protein	15.4
Acetate/ion	19.0/12.0
Water	30.8
r.m.s deviations	
Bond lengths (Å)	0.012
Bond angles (degrees)	1.554
Ramachandran statistics	
Favored (%)	98.9
Allowed (%)	0.5
Outlier (%)	0.5 (Gly^{373})

ing buffer. Collected protein eluate was analyzed by SDS-PAGE for purity, pooled, and used for biochemical assays following buffer dialysis to remove imidazole. Protein dedicated for crystallization trials was further processed by buffer exchanging into 20 mM Tris-HCl, pH 8.0, 2 mM $CaCl_2$ and treatment with 1.5 units of thrombin at room temperature overnight. The extent of protein cleavage was evaluated by SDS-PAGE, and then *Ye*OGL was concentrated in a stirred ultrafiltration device at 4 °C under nitrogen pressure. Protein was loaded onto an S-200 gel filtration column in 20 mM Tris-HCl to further purify the protein. The major protein peak was detected by UV absorbance, pooled, and concentrated to 12.5 mg/ml for crystallization trials.

Crystallization and Structure Solution—*Ye*OGL was screened for crystallization conditions using the hanging drop vapor diffusion method by mixing with an equal volume of mother liquor and incubating at 18 °C. Crystals formed in 0.2 M $CaCl_2$, 0.1 M NaOAc, pH 4.8, 20% PEG 3350 and were cryoprotected with 15% ethylene glycol. Diffraction data were collected at the Canadian Light Source on beamline CMCF1 and processed using iMOSFLM and SCALA (17) (see Table 1 for a list of data collection and refinement statistics). The structure was solved with PHASER (18), using the *Vibrio parahemeolyticus* homolog of *Ye*OGL (*Vp*OGL; Protein Data Bank entry 3C5M, 68% identity) as the search model. The *Ye*OGL model was corrected and completed by successive rounds of manual building in COOT (19) and refinement with REFMAC (20), all within the CCP4 suite of programs (21). Waters were added using the ARP/WARP option in REFMAC and then visually inspected prior to structure deposition. The final coordinates were validated with SFCHECK (22) and PROCHECK (23). The modeled GalA complex was constructed by exporting a monogalacturonate in an energy-minimized state from the Glycam Biomolecule Builder (24) and superimposing the uronate group with the ligated acetate ion. The monosaccharide was modeled with the axial O4 projecting toward solvent and H5 toward His^{242}, the closest basic amino acid in the active site with appropriate geometry for proton abstraction.

Kinetic Assays—Activity of *Ye*OGL on digalacturonate was first demonstrated using thin layer chromatography. Enzyme digests were set up with 0.1 μM enzyme and 1.0 mM substrate in Tris-HCl, pH 7.0 (a previously reported condition for *Ec*OGL (14)) and incubated for 10 min at 37 °C. At 0, 1, and 5 min, aliquots were removed and assayed for the formation of monosaccharide products by loading TLC silica gel plates with aluminum backing (EMD; 55553-7) and run in 1-butanol/acetic acid/water (2:1:1, v/v/v) solvent for 4 h. Plates were dried and developed using orcinol sulfuric acid reagent (sulfuric acid/ethanol, 3:70 (v/v), orcinol 1%). Sugars were visualized by heating. Activity of *Ye*OGL was quantified using wild-type enzyme at 0.5 μM and substrate concentrations ranging from 0.025 to 6.4 mM. The formation of product was monitored by absorbance at 230 nm. The highest concentration points had an inhibitory effect on activity, an effect commonly observed for pectate lyases (25), and were excluded from the Michaelis-Menten calculations. All assays for wild-type and catalytic mutants were performed in 0.1 mM Tris-HCl, pH 7.0, supplemented with 1.0 mM $MnCl_2$ at 25 °C. The molar extinction coefficient used to quantify DKI production (the unsaturated reaction product) was 4,600 M^{-1}

(26). Reactions were performed in triplicate for statistical significance, and the data were processed using GraphPad Prism® version 5 software.

Metal supplementation assays were performed as described for *Ye*PL2A (13). Each reaction series was run in triplicate for statistical accuracy. Control reactions were set up using 0.5 μM *Ye*OGL and 0.2 mM $GalA_2$ in 0.1 mM Tris-HCl, pH 7.0. Activities were ablated with 2 mM EDTA and recovered by the addition of a 10 mM divalent cation-chloride salt, which saturates the chelating agent on a molar basis (EDTA/metal, 5:2). In the presence of $MnCl_2$, the reaction rate was increased above that of the wild-type enzyme activity.

RESULTS AND DISCUSSION

Structure of YeOGL—Although the existence of OGLs has been known for some time, no representative structure has been reported in the literature, and thus the structural features that contribute to the function of these enzymes remained unknown. To explore the structural basis of OGL activity, we determined the high resolution x-ray crystal structure of *Ye*OGL. The entire 388 amino acids of OGL plus 572 water molecules, one manganese ion, two calcium ions, and one acetate ion (a component of the crystallization buffer) in bidentate coordination with the manganese ion are visible within the electron density (to be deposited in proof). The metal was determined to be Mn^{2+} based upon high resolution structural data supporting appropriate covalent coordination bond lengths, ligated nitrogen chemistry, coordination sphere symmetry, and anomalous signal (see below). *Ye*OGL adopts a seven-bladed β-propeller fold (Fig. 3) that has structural similarity to the WD40 family of proteins (27, 28). A DALI-Lite version 3 search (29) revealed the highest similarity to OGL from *V. parahemeolyticus* (*Vp*OGL), solved by the Northeast Structure Genomics initiative (Protein Data Bank entry 3C5M, *Z* value = 59.1, r.m.s. deviation = 1.1 Å, with 68% identity over 373 aligned amino acids), which was used as the search model to solve the structure of *Ye*OGL. Other than these two bacterial lyases, however, the closest structural homologs are proteins that display very little sequence and functional similarity. The next two closest hits belong to components of eukaryotic enzymes, including the Bα subunit of the protein phosphatase 2A holoenzyme (28) (Protein Data Bank entry 3DW8, *Z* value = 22.1, r.m.s. deviation = 3.2 Å, with 10% identity over 286 aligned amino acids) and the histone-binding protein RBBP7 (27) (Protein Data Bank code 3CFS, *Z* value = 22.1, r.m.s. deviation = 3.1 Å, with 10% identity over 290 aligned amino acids). These observations suggest that the seven-bladed β-propeller is a plastic fold capable of accommodating diverse functionalities.

Each propeller in *Ye*OGL consists of a repeating antiparallel four-stranded β-substructure (labeled A–D, using nomenclature described for other structural homologs) that flows from the core of the protein toward the outer surface of the protein (Fig. 3, *A* and *B*). The innermost strands (strand A) are connected to the outermost strand (strand D) of the preceding propeller by loops that vary greatly in length and structure and congregate on the upper surface of the protein, consistent with other seven-bladed propeller proteins (27, 28). One of these loop segments, a stretch of 11 amino acids connecting strands B and C of propeller 6 (Pro^{305}–Glu^{316}), could not be modeled because the density in this region was too poor. This is also observed in the structure of *Vp*OGL, suggesting that the absence of density is due to flexibility in this loop region rather than crystallographic packing effects. The "pinwheel-like" fold is capped at the C terminus by two N-terminal antiparallel strands (7C and 7D) that deviate from the contiguous repeating β-structures to form the two outer strands of the seventh propeller. The C-terminal sequence exits through the bottom of the protein and projects into solvent. The only noticeable α-helical structure (α1) is a 12-amino acid sequence (Asp^{154}–Lys^{165}) within the third propeller that lies on the protein surface.

The solvent-accessible electrostatic surface model of *Ye*OGL reveals that there is a prominent tunnel lined with basic amino acids burrowing from the surface toward a core metal binding site (Fig. 3*C*). Metal coordination pockets are a signature substructure within pectate lyases and a key feature of the β-elimination chemistry, highlighting that this is the location of the active site in *Ye*OGL. The walls of the tunnel are formed by several loop regions, an observation consistent with the active sites of other WD40 enzymes (27, 28), and capped by the α-helix (α1). Surprisingly, the tunnel appears to exit into solvent on both sides of the protein, reminiscent of the possessive cellobiohydrolase (30), as opposed to displaying a "pocket-like" structure more common within *exo*-acting enzymes (31). In the full-length *Ye*OGL, however, it is likely that the rear of the active site is occluded by the missing loop segment because the loop truncation occurs near this region. One entrance to the active site would require the substrate and product to access and depart the active site through the same portal.

The Unique Metal Binding Pocket of a Cytoplasmic Pectate Lyase—All described pectate lyase families utilize a catalytic metal during β-elimination of GalA. Mechanistically, uronate coordination contributes to electron delocalization and acidification of the α-proton at C5 of the aglycone sugar (Fig. 2). Calcium is the only metal that has been found in the active sites of extracellular lyases; interestingly, however, this metal also plays several other significant roles in the modification of pectic fragments and regulation of pectin ultrastructure. These include 1) the "egg box" model (32), a dynamic and physiologic process by which divalent cations cross-link the uronate groups, enabling the reversible gellation and solubilization of homogalacturonate chains, and 2) bridging substrate uronate groups and protein contact points at distal subsites within pectate lyases, interactions that contribute to the binding energy and substrate specificity. These reactions tend to be transient, however, and do not require an intact metal binding pocket in the absence of enzyme-substrate complexes. The prominent and diverse roles of calcium in pectinase activity and pectin structure may be linked to the prevalence of this metal cofactor within the plant cell wall (~1 mM).

By comparison with extracellular lyases, the more specialized role of catalytic metals in pectate lyases that operate within the confines of bacterial membranes has only just begun to be defined. The initial two cases revealed that two *E. chrysanthemi* (*D. dadantii Ech586*) enzymes, PelW (a family 2 PL) and *Ec*OGL (a family 22 PL), could harness novel metal cofactors,

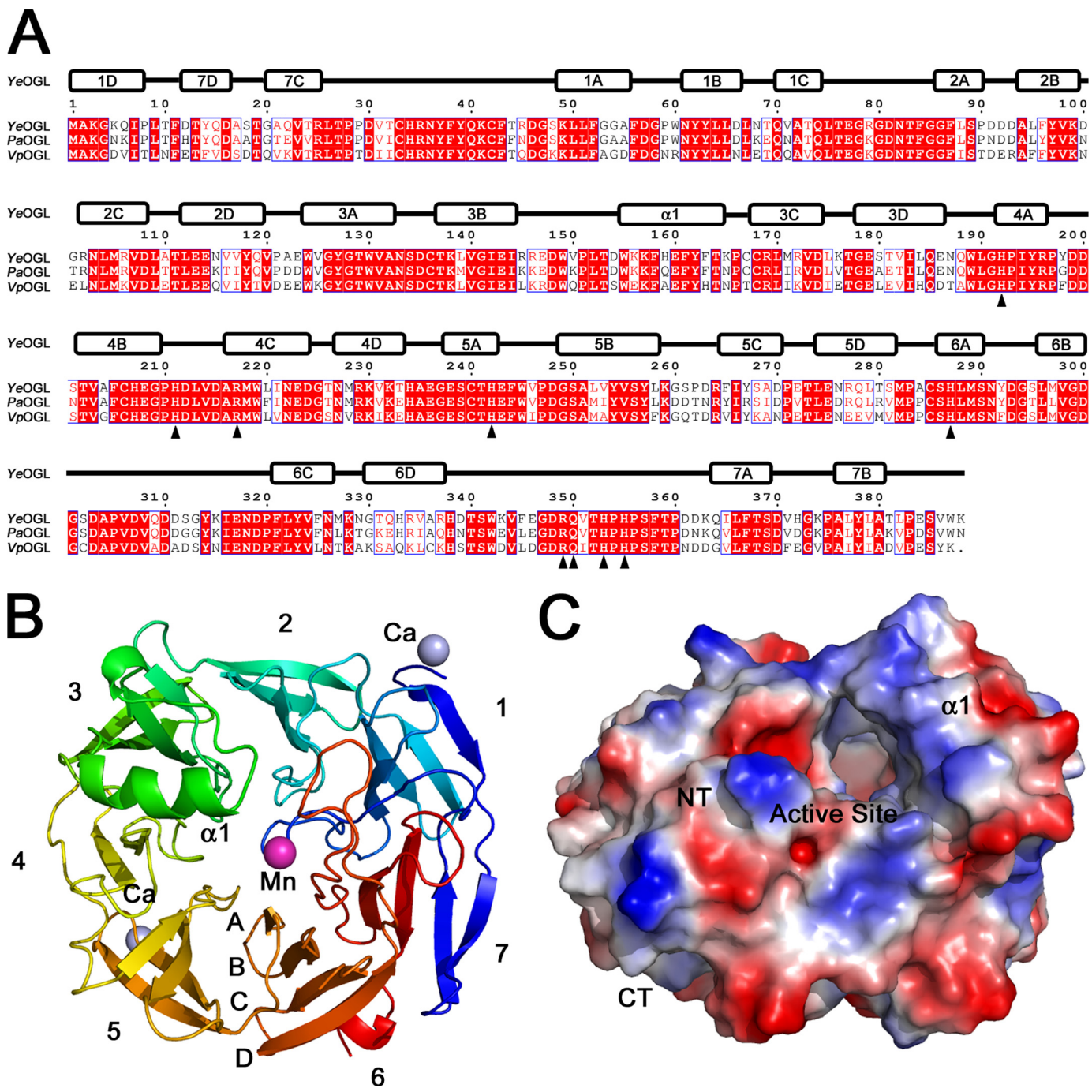

FIGURE 3. **β-Propeller fold of *Ye*OGL.** *A*, structural alignment of OGLs from *Y. enterocolitica* (*Ye*OGL), *E. chrysanthemi* (*Ec*OGL), and *V. parahemeolyticus* (*Vp*OGL). The secondary structure elements of *Ye*OGL are displayed *above* the aligned primary structure. Amino acids targeted for mutagenesis are indicated with *black triangles below* the sequences. *B*, schematic representation of *Ye*OGL structure colored from the N terminus (*blue*) to C terminus (*red*). The seven β-propellers are labeled (*1–7*) with each strand (*A–D*) packing from the core toward the surface. The three bound metal ions are displayed as *spheres* with the catalytic manganese *colored* in *purple* and the surface-bound calciums in *light blue*. *C*, electrostatic surface potential of *Ye*OGL. The protein is centered to display the entrance to the active site that is lined with several basic patches.

including manganese, nickel, and cobalt (14). In contrast to calcium, coordination of these transition metals requires signature nitrogen ligands presented by histidine residues (33). Recently, we provided a structure-function explanation for manganese coordination by two homologs of PelW from *Y. enterocolitica*, *Ye*PL2A and *Ye*PL2B (13). Within the coordination pocket of these enzymes, two histidine residues were identified that contribute to the octahedral geometry at distances consistent with the binding of manganese.

To further explore the emerging relationship between pectate lyase location and differential metal coordination chemistry, we have dissected the manganese binding pocket within *Ye*OGL. The coordination sphere is composed of three histidines (His^{287}, His^{353}, and His^{355}) and a glutamine (Gln^{350}) residue that display coordinate bond distances ranging from 2.1 to 2.2 Å for all six ligands, consistent with compositions and distances described for other manganese complexes (33). Gln^{350} was modeled with Oϵ as the donor atom and Nϵ hydrogen bond

contact with an ordered water. This is the most stable tautomeric form because Nϵ lacks a free electron pair for covalent coordinate bond formation. The remaining two atoms that complete the octahedral geometry were determined to be the oxygen atoms of an acetate carboxylate group, which is supported by B-factor and difference map analysis (see Table 2 and Fig. 4*A*). Acetate is a component of the crystallization buffer and mimics the chemistry of the GalA uronate group.

This analysis defines the third pectate lyase that coordinates Mn^{2+}, two of which are cytoplasmic (PL2B/OGL) and one of which is periplasmic (PL2A) (13, 14) (Fig. 1). These select enzymes contrast with the more abundant examples of extracellular secreted pectate lyases that exclusively utilize calcium. The molecular basis for the relationship between cellular distribution and metal selectivity had yet to be elucidated. Although the possibility of metals contributing different mechanistic effects to the reaction must be considered because calcium and transition metals display distinct electron orbital structures, it appears likely that this relationship may reflect the distribution of trace elements within prokaryotes. Although the roles of intracellular calcium in bacteria are still poorly understood, emerging evidence has revealed that, similar to eukaryotes, calcium is a signaling molecule in many bacterial processes, such as transport, cell differentiation, and the maintenance of cell structure (34, 35). As a result, calcium levels within the cell are limiting and tightly regulated (100–300 nM) (36, 37). Therefore, intracellular pectate lyases may have evolved unique chemistries tailored for the coordination of metal cofactors (Mn^{2+} as opposed to Ca^{2+}) that are available in sufficient concentrations within the microenvironment in which they function. The observation that PL2A utilizes manganese and is operational within the periplasm, however, provides an interesting twist on this possibility because the calcium-utilizing pectate lyase, PelX (PL9), has also been determined to be functional within the periplasm (7, 38). Analysis of the primary structure of the intact *Ye*PL2A polypeptide reveals the presence of a signature Lys-Arg dipeptide in its secretion signal. This sequence marker indicates that *Ye*PL2A is folded within the cytoplasm and subsequently transported intact through a TAT pathway across the inner membrane (39, 40). *Y. enterocolitica* lacks a PelX homolog and therefore may have diversified its collection of pectinases by evolving to secrete a PL2 homolog that would be active in the upstream stages of the pathway. These enzymes are observed in only a few pectinolytic microbes; however, in almost every case, they are found in tandem PL2A and PL2B pairs (see the CAZy Web site) (7). Typically secreted pectinases transit through a SEC-mediated pathway in an unfolded state and therefore would incorporate a catalytic metal within a folding microenvironment where calcium is prevalent. This observation is reminiscent of the targeted folding and selective metal acquisition of the *Synechocystis* metalloproteins MncA and CucA (41).

TABLE 2
Atomic distances and temperature factors for the manganese coordination pocket of *Ye*OGL

Ligand	Distance	*B*-Factor	Occupancy
	Å	*Å²*	
Mn		7.5	1.0
Nϵ-His^{287}	2.1	9.5	1.0
Oϵ-Gln^{350}	2.2	10.2	1.0
Nδ-His^{353}	2.2	8.7	1.0
Nδ-His^{355}	2.1	8.3	1.0
OA-ACT	2.1	17.0	1.0
OB-ACT	2.3	16.2	1.0

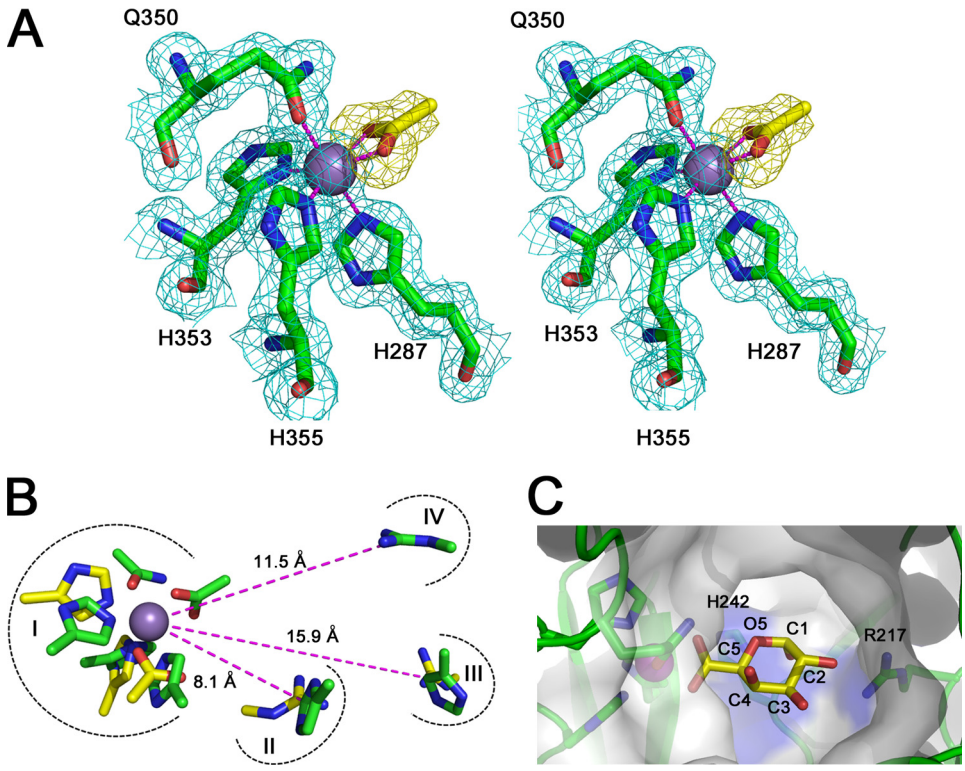

FIGURE 4. **The active site of *Ye*OGL.** *A*, the octahedral metal binding site is displayed in *wall-eyed stereo format* with the weighted maximum likelihood (20)/σ_A (53) $2F_o - F_c$ map (*cyan*) contoured to 1.0 σ (0.43 $e^-/Å^3$). The coordinated acetate ion (*yellow sticks*) is shown with an $F_o - F_c$ omit map, produced from phases generated during refinements with the acetate molecule excluded from the model, contoured at 2.5 σ (0.18 $e^-/Å^3$). This map demonstrates the high quality of unbiased electron density for this molecule. The three histidines (His^{287}, His^{353}, and His^{355}) and glutamine (Gln^{350}) are shown in *stick representation*, and the Mn^{2+} ion is modeled as a *sphere*. *B*, superimposition of catalytic substructures within the active site of *Ye*PL2A (*yellow*, Protein Data Bank entry 2V8J) and *Ye*OGL (*green*). Four aligned regions are shown: metal coordination pocket (*I*), catalytic base (*II*), and potential residues involved in substrate stabilization (*III* and *IV*). Distances of the residues from the metal are labeled. *C*, *cut-away surface representation* of the active site with a GalA modeled in the +1 subsite. The GalA uronate group of the aglycone is superimposed with the coordinated acetate ion with the axial H5 pointing toward the candidate Brønstead base His^{242} and O2 pointing toward the stabilizing Arg^{217}, and O4 is presented for polymerization.

Structural Analysis of the YeOGL β-Elimination Machinery—Evolutionary convergence of the catalytic machinery in pectate lyases has been observed in families 1, 2, and

10 (13, 42). Although these enzymes have no sequence relatedness and adopt unique folds, they display a constellation of functional residues within their active site that is structurally conserved. These include the components of the metal binding pocket involved in α-proton acidification; a basic residue, typically an arginine, which operates as the Brønstead base during H5 abstraction; and a secondary arginine that flanks the substrate by binding to its C2 and C3 hydroxyl groups. Therefore, based upon this premise and in order to dissect the molecular basis of β-elimination within the active site of *Ye*OGL, we have explored the evidence for structural convergence between *Ye*OGL and *Ye*PL2A. These two enzymes, unrelated at the sequence level, represent the only two characterized pectate lyases available in the data base in complex with a Mn^{2+} ion. Comparing the active sites of these two lyases is complicated by the presence of the two alternate conformations of *Ye*PL2A that have been described, which represent distinct structural snapshots across the catalytic landscape of the enzyme. The Mn^{2+} complex, or "open" form, is poised for substrate binding; whereas the $GalA_3$-Michaelis complex, or "closed" form, has locked its two catalytic arms around the substrate, resulting in a rearrangement of the core β-elimination machinery (13). The lack of a metal in the *Ye*PL2A-$GalA_3$ complex results in a shift of the substrate orientation within the active site because the uronate group is not anchored by coordination. Preliminary rounds of analysis determined that the metal-bound complex of *Ye*OGL and *Ye*PL2A (with both enzymes lacking sugar substrate) display the greatest level of structural similarity in the alignment of their catalytic residues. Therefore, in the following discussion, we will describe the superimposition of the two active sites using the metal as a central reference point.

Four main substructures were identified (I–IV) (Fig. 4*B*). In I, the metal binding site shares several structurally conserved donor atoms within both enzymes, including two histidines. Interestingly, the Gln^{350} of *Ye*OGL did not align with any candidate residues from *Ye*PL2A. This glutamine, which also binds an ordered water molecule, may be functionally similar to the catalytic amides from family PL9 and PL10 lyases. It has been proposed that amide groups proximal to the uronate may stabilize the enolate-enolate intermediate through hydrogen bonding (42, 43) (Fig. 2). In II, the Brønstead base from *Ye*PL2A (Arg^{171}) structurally aligns with His^{242} in *Ye*OGL, the only basic residue with suitable proximity and geometry for abstracting the H5 of a bound GalA substrate. Histidine-catalyzed β-elimination has been proposed for the family PL8 *Streptcoccus pneumoniae* hyaluronate lyase (SpPL8) (44); however, to the best of our knowledge, this is the first description of a similar role for this residue in pectate lyases. The remaining two substructures, III and IV, represent two potential substrate stabilizing residues in *Ye*OGL. In III, the His^{211} in *Ye*OGL superimposes well with the Arg^{272} of *Ye*PL2A in its open conformation; however, this position is distal to the metal binding site (~15.9 Å) and in an unfavorable position to interact directly with the substrate. In *Ye*PL2A, this is explained through a change in enzyme conformation; following $GalA_3$ binding, Arg^{272} undergoes a positional shift of 4.4 Å toward the aglycone sugar. Further analysis of the *Ye*OGL structure reveals that the arginine displayed in IV (Arg^{217}) most likely interacts with GalA in subsite +1 (bond cleavage occurs between the sugars at subsites −1 and +1) based upon its configuration because both Nη of the guanidine group are pointing toward the metal binding pocket, consistent with other pectate lyase structures, functional group chemistry, and proximity. In *Ye*OGL, the two Arg^{217} nitrogen atoms are 11.2 and 11.5 Å, respectively from the coordinated metal, which is very similar to the distances between the guanidine group of Arg^{272} (10.9 and 11.0 Å) and a bound water molecule in the $GalA_3$-Michaelis complex of *Ye*PL2A (not shown). This observation suggests that there is more conformational flexibility within the active site of *Ye*PL2A than *Ye*OGL and that the active site of *Ye*OGL presents another strong example of the structural convergence of the β-elimination machinery in pectate lyases. The potential role of this highly conserved arginine in catalytic proton transfer to the glycosidic oxygen of the scissile bond, in *Ye*OGL and other pectate lyases, remains to be established (42, 45).

Crystallographic investigations into the molecular basis of *Ye*OGL recognition of oligogalacturonides have proven unsuccessful. Fortuitously, however, the coordination of an acetate molecule to the Mn^{2+} ion provides a framework for predicting the position of a GalA molecule within the active site (Fig. 4*C*). A *Ye*OGL-GalA model was constructed by superposing the uronate group of GalA with the bound acetate group. To select between the two possible orientations, the monosaccharide was positioned such that the axial hydrogen is pointing toward the candidate Brønstead base, His^{242}, as opposed to toward the top of the active site, a region lacking any definable basic residue suitable for potential proton abstraction. In this configuration, the O2 hydroxyl of GalA is directed toward the guanidine group of Arg^{217}. Although the model does not account for subtle changes in conformation and orientation that may be induced by binding energy, the two molecules are already approaching hydrogen bond distance. O1 is pointing toward the core of the enzyme and the rear exit of the solvent tunnel, and the axial O4 is positioned toward the tunnel entrance to accommodate polymerization of another GalA. Based upon these observations, it is likely that in the native complex, GalA undergoes a small rotation around its planar axis so that O2 and O3 both interact with Arg^{217}, and O4 extends closer toward the center of the solvent tunnel to alleviate any steric clash with the wall of the enzyme.

Transition Metal Utilization by YeOGL—to test the viability of our model and interrogate the role of Mn^{2+} in the elimination of oligogalacturonate, we have characterized the active site by enzyme kinetics and metal supplementation assays. Preliminary assays revealed that *Ye*OGL is active on $GalA_2$ (Fig. 5*A*). Calculated kinetic values (see Fig. 5*B* and Table 3) suggest that *Ye*OGL has an activity identical to that of its *Ec*OGL homolog (14), a result that is not surprising when considering the high level of amino acid conservation between the two proteins. The ~8-fold higher maximal velocity of *Ye*OGL on $GalA_2$ ($43.67 \pm 5.16\ min^{-1}$) compared with $GalA_3$ ($5.70 \pm 0.49\ min^{-1}$), underpins the complementary role of *Ye*PL2B/PelW. *Ye*PL2B/PelW is dedicated to the conversion of cytoplasmic trisaccharides into substrates for OGL, a process that will ultimately increase the efficiency of the upstream stages of cytoplasmic oligogalacturonide catabolism (see Fig. 1). Previously, a cluster of transi-

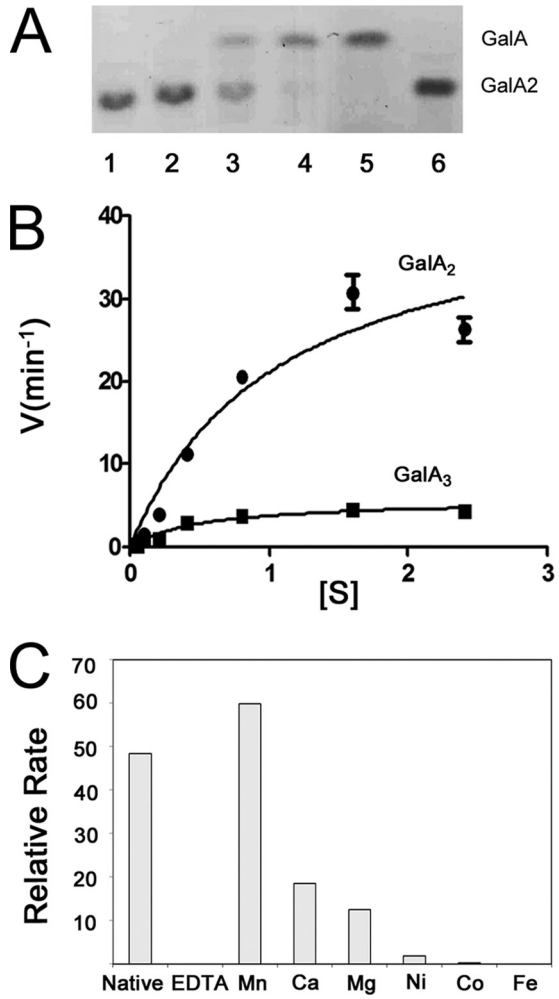

FIGURE 5. **Activity of *Ye*OGL.** *A*, TLC gel of $GalA2_2$ digestion. Lanes are loaded as follows: no enzyme control (*lane 1*), increasing reaction time points (0–5 min) (*lanes 2–4*), GalA standard (*lane 5*), and $GalA_2$ standard (*lane 6*). *B*, reaction rates are plotted with velocity (min^{-1}) against substrate concentration (mM). *C*, metal supplementation assays. Rates shown represent quantified changes in UV absorbance. *Error bars*, S.D.

TABLE 3
Kinetic values of *Ye*OGL

Substrate	K_m	K_{cat}	K_{cat}/K_m
	mM	min^{-1}	$min^{-1}\ mM^{-1}$
$GalA_2$	1.07 ± 0.28[a]	43.67 ± 5.16	40.81
$GalA_3$	0.52 ± 1.2	5.70 ± 0.49	10.96

[a] S.D. values are based upon the rate calculations for three independently performed experiments.

tion metals, ranging from the seventh to the tenth row of the fourth period, were previously shown to be capable of assisting in the catalytic activity of *Ec*OGL to varying degrees ($Mn^{2+} > Co^{2+} > Fe^{2+} > Ni^{2+}$) (14). This finding indicated that the metal-coordinating machinery of this lyase family is tailored to utilizing transition metals. Similar recovery assays performed for *Ye*OGL also revealed a preferential relationship with Mn^{2+} because other cofactors failed to restore similar levels of enzyme activity (Fig. 5*C*). These assays support the structural observations for tailored metal binding within the OGL family discussed above.

*Evolution of the OGL Family—Ec*OGL was first discovered in 1968 (originally referred to as oligogalacturonide transeliminase (46)) and known to be found in diverse species of Enterobacteriaceae, including *Y. enterocolitica*, for over a decade (8); however, a detailed analysis of the relatedness of orthologs and its classification as a novel polysaccharide lyase family in the CAZy data base has been lacking. Therefore, to provide insight into the functional relatedness of the family, we did a BLAST search using the *Ye*OGL as a query sequence. Initial searches identified 46 family members (with a low end cut-off value of ≥10 for several outlying sequences as determined in the Carbohydrate-Active Enzymes Database)[5] that partition into two clusters, one of which contains ~85% of the entries (relatedness value of 53–97%), including the characterized enzymes from *E. chrysanthemi* (CAA43990) and *Y. enterocolitica* (CAL11955) and the uncharacterized structural homolog from *V. parahemeolyticus* (BAC61431). The smaller seven-member outgroup (relatedness threshold value of 10–52%) consists of uncharacterized putative enzymes from *Candidatus Solibacter usitatus* (ABJ83750, ABJ85020, and ABJ83823), *Roseiflexus castenholizii* (ABU58452 and ABU58528), and single entries from *Geobacillus sp.* and *Haloterrigena turkmenica*. The presence of OGL in each of these species indicates that these microorganisms have a propensity to utilize pectin as an energy source.

To compare the functional residues across the OGL family, a ClustalW alignment (47) was performed on sequences from each representative species; redundant entries from individual strains were omitted for clarity (Fig. 6). There is high level sequence conservation across the entire family. Inspection of the putative catalytic histidine (H242) and stabilizing arginine (R217) reveals that they are virtually invariant. Only one sequence (ABJ83823) from *S. usitatus* displays unique residues at these positions, which in addition contains a completely remodeled metal binding site and raises the question of whether it is even a functional lyase. Closer analysis of the other two entries from *S. usitatus* (ABJ83750 and ABJ85020) may provide insight into the potential relationship between metal selectivity and cellular localization we have described above. Both of these putative enzymes contain *bona fide* signal peptides. The lack of a consensus TAT sequence (not shown) suggests that they are targeted for a general secretion pathway and therefore are folded outside the cytoplasm, where Ca^{2+} is abundant. Closer investigation of catalytic machinery in these homologs reveals that they contain the putative catalytic histidine; however, noticeable substitutions are present within the metal binding site. The His^{353} and His^{355} from *Ye*OGL are replaced with a glutamate and asparagine residue, respectively. These functional groups contribute oxygen donor atoms during coordinate bond formation, indicating a potential loss of Mn^{2+} and gain of Ca^{2+} binding specificity. In addition, although His^{287} is conserved in the primary structure, it is located in a stretch of amino acids displaying very little similarity in the *S. usitatus* proteins, and therefore, it is difficult to justify a spatial and functional conservation of the histidine at this site. These two predicted enzymes from the OGL family, therefore, provide further support for the hypothesis that pectate lyase catalytic metal selectivity is based upon the location of enzyme folding rather than mechanistic effects.

[5] B. Henrissat and P. M. Coutinho, personal communication.

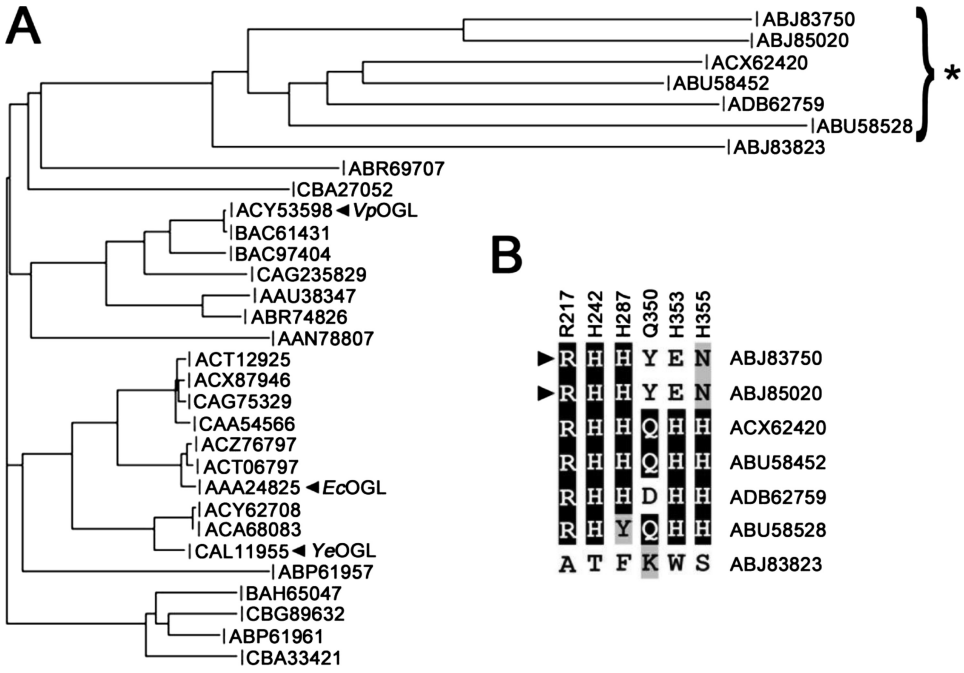

FIGURE 6. **Pylogenetic tree of the OGL family.** Related sequence targets are shown as a *phylogram*. The out-group is indicated with an *asterisk*. The *inset* displays the level of conservation of functional residues for the seven out-group sequences, and the putative secreted pectate lyases are indicated with *black triangles*.

The observation that *Yersinia pestis*, the causative agent of the bubonic plague, possesses an OGL homolog is intriguing. In addition to this cytoplasmic lyase, the genome of every known *Y. pestis* strain was shown to contain genetic evidence of a well developed pectin utilization pathway (7) (see the CAZy Web site). These observations appear inconsistent with traditional life cycle models of the pathogen because *Y. pestis* is widely considered an enzootic disease and is not known to colonize the digestive tract of its mammalian host. It is difficult to rationalize therefore where the microbe would have access to dietary pectin and concomitantly why it would contain a pathway tailored to its catabolism. Recently, however, it has been reported that *Y. pestis* can persist within soil (48–50), a process that may be facilitated by scavenging dietary carbohydrates, such as pectin. Utilizing plant cell wall polysaccharides as a transient energy source may explain the mechanistic basis of how *Y. pestis* lies dormant within and passages through the environment as it waits for an opportunity to colonize new host reservoirs. This possibility awaits further investigation, however, because the presence of pectin utilization genes within *Y. pestis* may more simply reflect the evolutionary history of this genus, and this pathway may in fact be a decommissioned remnant containing non-functional enzymes.

CONCLUSION

Early structural analysis suggested that PLs harness a structurally conserved β-helix fold to modify and dismantle pectin (51, 52). Structural biology within the past decade, however, has illuminated the great structural diversity in protein folds that actually exists within nature for this class of carbohydrate-active enzymes (this work and see Refs. 13 and 42). Analysis of the catalytic substructures within diverse PL families has established a new paradigm for our understanding of PL structure-function relationships: the remarkable structural convergence of active site chemistry. Tailoring distinct protein scaffolds with highly similar catalytic apparatus strongly suggests that the β-elimination machinery and the stereochemical identity of their target substrate place heavy selective pressure on the evolutionary processes driving the structural convergence of these enzyme families. Beyond the core features of the PL active site, however, several variations on this theme have begun to surface with the increase of available structural information. First, it appears that the OGL family utilizes a histidine as a Brønstead base during H5 abstraction. Outside of family 9 pectate lyases, which utilize a lysine, all other described examples exclusively display catalytic arginines. The significance of this chemical substitution probably reflects the localized OGL environment. Indeed, the optimal pH of *Ye*OGL is between 7.3 and 7.7 (*Ec*OGL (14); *Ye*OGL not shown), consistent with the buffered solution of the bacterial cell. Additionally, this pH optimum is more alkaline than the pK_a of histidine (pK_a = 6.1), an observation that contrasts with that of extracellular lyases. Secreted enzymes display a pH optimum around 9.0 (25), which requires localized pK_a effects perturbing the catalytic arginine (pK_a = 12.5) to display a more acidic character. Second, the metal binding site of *Ye*OGL possesses three histidines and a glutamine, tailored for the coordination of Mn^{2+}. This is the second lyase, representing two different PL families with unique protein folds, that harnesses a metal cofactor other than calcium. What distinguishes these two enzyme families from previous complexes is that *Ye*OGL and *Ye*PL2B are cytoplasmic lyases and therefore fold and operate in an environment that limits the availability of calcium ions. The periplasmic homolog of *Ye*PL2B, *Ye*PL2A, contains a TAT secretion signal in its signal peptide, indicating that it is folded within the cell and secreted into the periplasm intact. This observation suggests that it is the environment in which the enzyme is folded that dictates the metal cofactor selection within the active site of pectate lyases and not the mechanistic influences.

As the field continues to advance, it will be exciting to discover whether the vast arsenal of uncharacterized pectate lyases encoded within the distal gut microbiome also display structural convergence in the architecture of their catalytic site and a metal selectivity dependent on cellular localization or if this dynamic and densely populated community has evolved novel platforms for the β-elimination of pectate.

Acknowledgments—We thank B. Henrissat and P. M. Coutinho for assistance in defining the cut-off parameters for the OGL family.

REFERENCES

1. Bäckhed, F., Ley, R. E., Sonnenburg, J. L., Peterson, D. A., and Gordon, J. I. (2005) *Science* **307,** 1915–1920
2. Martens, E. C., Koropatkin, N. M., Smith, T. J., and Gordon, J. I. (2009) *J. Biol. Chem.* **284,** 24673–24677
3. O'Hara, A. M., and Shanahan, F. (2006) *EMBO Rep.* **7,** 688–693
4. Sonnenburg, J. L., Xu, J., Leip, D. D., Chen, C. H., Westover, B. P., Weatherford, J., Buhler, J. D., and Gordon, J. I. (2005) *Science* **307,** 1955–1959
5. Martens, E. C., Roth, R., Heuser, J. E., and Gordon, J. I. (2009) *J. Biol. Chem.* **284,** 18445–18457
6. Martens, E. C., Chiang, H. C., and Gordon, J. I. (2008) *Cell Host Microbe* **4,** 447–457
7. Rodionov, D. A., Gelfand, M. S., and Hugouvieux-Cotte-Pattat, N. (2004) *Microbiology* **150,** 3571–3590
8. Rodionov, D. A., Mironov, A. A., Rakhmaninova, A. B., and Gelfand, M. S. (2000) *Mol. Microbiol.* **38,** 673–683
9. Caffall, K. H., and Mohnen, D. (2009) *Carbohydr. Res.* **344,** 1879–1900
10. Mohnen, D. (2008) *Curr. Opin. Plant Biol.* **11,** 266–277
11. Abbott, D. W., and Boraston, A. B. (2008) *Microbiol. Mol. Biol. Rev.* **72,** 301–316, table of contents
12. Hugouvieux-Cotte-Pattat, N., Condemine, G., Nasser, W., and Reverchon, S. (1996) *Annu. Rev. Microbiol.* **50,** 213–257
13. Abbott, D. W., and Boraston, A. B. (2007) *J. Biol. Chem.* **282,** 35328–35336
14. Shevchik, V. E., Condemine, G., Robert-Baudouy, J., and Hugouvieux-Cotte-Pattat, N. (1999) *J. Bacteriol.* **181,** 3912–3919
15. Cantarel, B. L., Coutinho, P. M., Rancurel, C., Bernard, T., Lombard, V., and Henrissat, B. (2009) *Nucleic Acids Res.* **37,** D233–D238
16. Boraston, A. B., Creagh, A. L., Alam, M. M., Kormos, J. M., Tomme, P., Haynes, C. A., Warren, R. A., and Kilburn, D. G. (2001) *Biochemistry* **40,** 6240–6247
17. Evans, P. (2006) *Acta Crystallogr. D Biol Crystallogr.* **62,** 72–82
18. McCoy, A. J., Grosse-Kunstleve, R. W., Adams, P. D., Winn, M. D., Storoni, L. C., and Read, R. J. (2007) *J. Appl. Crystallogr.* **40,** 658–674
19. Emsley, P., and Cowtan, K. (2004) *Acta Crystallogr. D Biol. Crystallogr.* **60,** 2126–2132
20. Murshudov, G. N., Vagin, A. A., and Dodson, E. J. (1997) *Acta Crystallogr. D Biol. Crystallogr.* **53,** 240–255
21. Potterton, L., McNicholas, S., Krissinel, E., Gruber, J., Cowtan, K., Emsley, P., Murshudov, G. N., Cohen, S., Perrakis, A., and Noble, M. (2004) *Acta Crystallogr. D Biol. Crystallogr.* **60,** 2288–2294
22. Vaguine, A. A., Richelle, J., and Wodak, S. J. (1999) *Acta Crystallogr. D Biol. Crystallogr.* **55,** 191–205
23. Laskowski, R. A., MacArthur, M. W., Moss, D. S., and Thornton, J. M. (1993) *J. Appl. Crystallogr.* **26,** 283–291
24. Kirschner, K. N., Yongye, A. B., Tschampel, S. M., González-Outeiriño, J., Daniels, C. R., Foley, B. L., and Woods, R. J. (2008) *J. Comput. Chem.* **29,** 622–655
25. Tardy, F., Nasser, W., Robert-Baudouy, J., and Hugouvieux-Cotte-Pattat, N. (1997) *J. Bacteriol.* **179,** 2503–2511
26. Scavetta, R. D., Herron, S. R., Hotchkiss, A. T., Kita, N., Keen, N. T., Benen, J. A., Kester, H. C., Visser, J., and Jurnak, F. (1999) *Plant Cell* **11,** 1081–1092
27. Murzina, N. V., Pei, X. Y., Zhang, W., Sparkes, M., Vicente-Garcia, J., Pratap, J. V., McLaughlin, S. H., Ben-Shahar, T. R., Verreault, A., Luisi, B. F., and Laue, E. D. (2008) *Structure* **16,** 1077–1085
28. Xu, Y., Chen, Y., Zhang, P., Jeffrey, P. D., and Shi, Y. (2008) *Mol. Cell* **31,** 873–885
29. Holm, L., Kääriäinen, S., Rosenström, P., and Schenkel, A. (2008) *Bioinformatics* **24,** 2780–2781
30. Rouvinen, J., Bergfors, T., Teeri, T., Knowles, J. K., and Jones, T. A. (1990) *Science* **249,** 380–386
31. Davies, G., and Henrissat, B. (1995) *Structure* **3,** 853–859
32. Liners, F., Letesson, J. J., Didembourg, C., and Van Cutsem, P. (1989) *Plant Physiol.* **91,** 1419–1424
33. Harding, M. M. (2001) *Acta Crystallogr. D Biol. Crystallogr.* **57,** 401–411
34. Dominguez, D. C. (2004) *Mol. Microbiol.* **54,** 291–297
35. Michiels, J., Xi, C., Verhaert, J., and Vanderleyden, J. (2002) *Trends Microbiol.* **10,** 87–93
36. Gangola, P., and Rosen, B. P. (1987) *J. Biol. Chem.* **262,** 12570–12574
37. Gilroy, S., Fricker, M. D., Read, N. D., and Trewavas, A. J. (1991) *Plant Cell* **3,** 333–344
38. Shevchik, V. E., Kester, H. C., Benen, J. A., Visser, J., Robert-Baudouy, J., and Hugouvieux-Cotte-Pattat, N. (1999) *J. Bacteriol.* **181,** 1652–1663
39. DeLisa, M. P., Samuelson, P., Palmer, T., and Georgiou, G. (2002) *J. Biol. Chem.* **277,** 29825–29831
40. De Buck, E., Lammertyn, E., and Anné, J. (2008) *Trends Microbiol.* **16,** 442–453
41. Tottey, S., Waldron, K. J., Firbank, S. J., Reale, B., Bessant, C., Sato, K., Cheek, T. R., Gray, J., Banfield, M. J., Dennison, C., and Robinson, N. J. (2008) *Nature* **455,** 1138–1142
42. Charnock, S. J., Brown, I. E., Turkenburg, J. P., Black, G. W., and Davies, G. J. (2002) *Proc. Natl. Acad. Sci. U.S.A.* **99,** 12067–12072
43. Jenkins, J., Shevchik, V. E., Hugouvieux-Cotte-Pattat, N., and Pickersgill, R. W. (2004) *J. Biol. Chem.* **279,** 9139–9145
44. Li, S., Kelly, S. J., Lamani, E., Ferraroni, M., and Jedrzejas, M. J. (2000) *EMBO J.* **19,** 1228–1240
45. Seyedarabi, A., To, T. T., Ali, S., Hussain, S., Fries, M., Madsen, R., Clausen, M. H., Teixteira, S., Brocklehurst, K., and Pickersgill, R. W. (2010) *Biochemistry* **49,** 539–546
46. Moran, F., Nasuno, S., and Starr, M. P. (1968) *Arch. Biochem. Biophys.* **125,** 734–741
47. Thompson, J. D., Higgins, D. G., and Gibson, T. J. (1994) *Nucleic Acids Res.* **22,** 4673–4680
48. Ayyadurai, S., Houhamdi, L., Lepidi, H., Nappez, C., Raoult, D., and Drancourt, M. (2008) *Microbiology* **154,** 2865–2871
49. Drancourt, M., Houhamdi, L., and Raoult, D. (2006) *Lancet Infect. Dis.* **6,** 234–241
50. Eisen, R. J., Petersen, J. M., Higgins, C. L., Wong, D., Levy, C. E., Mead, P. S., Schriefer, M. E., Griffith, K. S., Gage, K. L., and Beard, C. B. (2008) *Emerg. Infect. Dis.* **14,** 941–943
51. Jenkins, J., and Pickersgill, R. (2001) *Prog. Biophys. Mol. Biol.* **77,** 111–175
52. Jenkins, J., Mayans, O., and Pickersgill, R. (1998) *J. Struct. Biol.* **122,** 236–246
53. Read, R. J. (1986) *Acta Crystallogr. A* **42,** 140–149